Title: Experimental study of smog microphysical and optical vertical structure in the Silesian Beskids, Poland

Author: Michał A. Posyniak, Krzysztof M. Markowicz, Dominika Czyżewska, Michał T. Chiliński, Przemysław Makuch, Olga Zawadzka-Mańko, S. Kucięba, Kinga Kulesza, Kamil Kachniarz, K .Mijal, Karolina Borek

Citation style: Posyniak Michał A., Markowicz Krzysztof M., Czyżewska Dominika, Chiliński Michał T., Makuch Przemysław, Zawadzka-Mańko Olga, Kucięba S., Kulesza Kinga, Kachniarz Kamil, Mijal K., Borek Karolina. (2021). Experimental study of smog microphysical and optical vertical structure in the Silesian Beskids, Poland. „Atmospheric Pollution Research" (Vol. 12, iss. 9, 2021, art. no. 101171, s. 1-11), DOI: 10.1016/j.apr.2021.101171

Atmospheric Pollution Research 12 (2021) 101171

Contents lists available at ScienceDirect

Atmospheric Pollution Research

journal homepage: www.elsevier.com/locate/apr

Experimental study of smog microphysical and optical vertical structure in the Silesian Beskids, Poland

M.A. Posyniak [a,*], K.M. Markowicz [b], D. Czyzewska [b,c], M.T. Chilinski [d], P. Makuch [e], O. Zawadzka-Manko [b], S. Kucieba [a], K. Kulesza [f], K. Kachniarz [g], K. Mijal [b], K. Borek [b]

[a] Institute of Geophysics, Polish Academy of Sciences, Ksiecia Janusza 64, Warsaw, 01-453, Poland
[b] Institute of Geophysics, Faculty of Physics, University of Warsaw, Pasteura 5, Warsaw, 02-093, Poland
[c] European Organisation for the Exploitation of Meteorological Satellites, Eumetsat Allee 1, Darmstadt, 64295, Germany
[d] Faculty of Biology, University of Warsaw, Miecznikowa 1, Warsaw, 02-096, Poland
[e] Institute of Oceanology, Polish Academy of Sciences, Powstancow Warszawy 55, Sopot, 81-712, Poland
[f] Institute of Physical Geography, Faculty of Geography and Regional Studies, University of Warsaw, Krakowskie Przedmiescie 30, Warsaw, 00-927, Poland
[g] Centre for Polar Studies, Institute of Earth Sciences, University of Silesia in Katowice, Bedzinska 60, Sosnowiec, 41-200, Poland

ARTICLE INFO

Keywords:
Max 6) black carbon
Vertical profile
Cable car
aerosol optical depth
Single scattering albedo
aerosol mass concentration

ABSTRACT

This study presents the vertical profiles of aerosol optical and microphysical properties obtained from cable car and ground-based measurements in the Silesian Beskids, Poland. The data were collected during a measurement campaign between 25 February and March 11, 2018. An AE-51 micro-aethalometer and PMS7003 and OPC-N2 optical particle counters were mounted on the cable car and used to measure the profiles of equivalent of black carbon (eBC) concentration and aerosol size distribution. In situ measurements of the optical properties of the aerosols were obtained using an AE-31 aethalometer and photoacoustic devices. A prototype lidar was used to determine the planetary boundary layer (PBL) height and the aerosol layers. In the middle phase of the study (1–6 March 2018), significant night-time temperature inversions were observed. During the inversion period, the parameters describing the amount of aerosols in the air increased significantly. The concentration of eBC exceeded the level of 15 μg/m^3 several times, with an average level of 5.39 ± 4.42 μg/m^3. Conversely, the results obtained in the first and third phases of the experiment were at the level of the aerosol background, being 1.45 ± 0.88 μg/m^3 and 0.90 ± 0.95 μg/m^3, respectively. Significant differences were also observed in the vertical profiles of PM_{10} mass and eBC concentration. In the middle phase of the study, the profiles showed a significant reduction in the concentration of pollutants with height, while in the first and third phases, there were slight variations with height.

1. Introduction

The emission of atmospheric aerosols, in combination with the processes of deposition and mixing, affects the concentration of particles in the lower troposphere (Colbeck and Lazaridis, 2010). The processes of mixing air in the horizontal plane (advection air mass) and in the vertical direction (the convection associated with the vertical temperature gradient in the atmosphere) drive the accumulation of particulate air pollutants (aerosols) at the ground level (Li et al., 2015, 2019; Wang et al., 2018). Moreover, topography influences the local air circulation and turbulence in the lower boundary layer, contributing to high concentrations of air pollutants at the surface (Okamoto and Tanimoto, 2016; Zhang et al., 2018).

In Poland, particularly during the autumn-winter season, emissions from residential heating and, to a lesser extent, from transport, are the main sources of particulate matter (Wielgosinski and Czerwinska, 2020). Smog forms because as a result of its high concentration. Although in recent years, a slow reduction in the level of air pollution has been observed in Poland (Markowicz et al., 2019), air quality in many regions remains poor.

To broaden the knowledge of aerosol optical and microphysical properties (Liu et al., 2014), researchers have employed both remote

Peer review under responsibility of Turkish National Committee for Air Pollution Research and Control.
* Corresponding author.
E-mail address: mpos@igf.edu.pl (M.A. Posyniak).

https://doi.org/10.1016/j.apr.2021.101171
Received 5 February 2021; Received in revised form 13 August 2021; Accepted 13 August 2021
Available online 16 August 2021

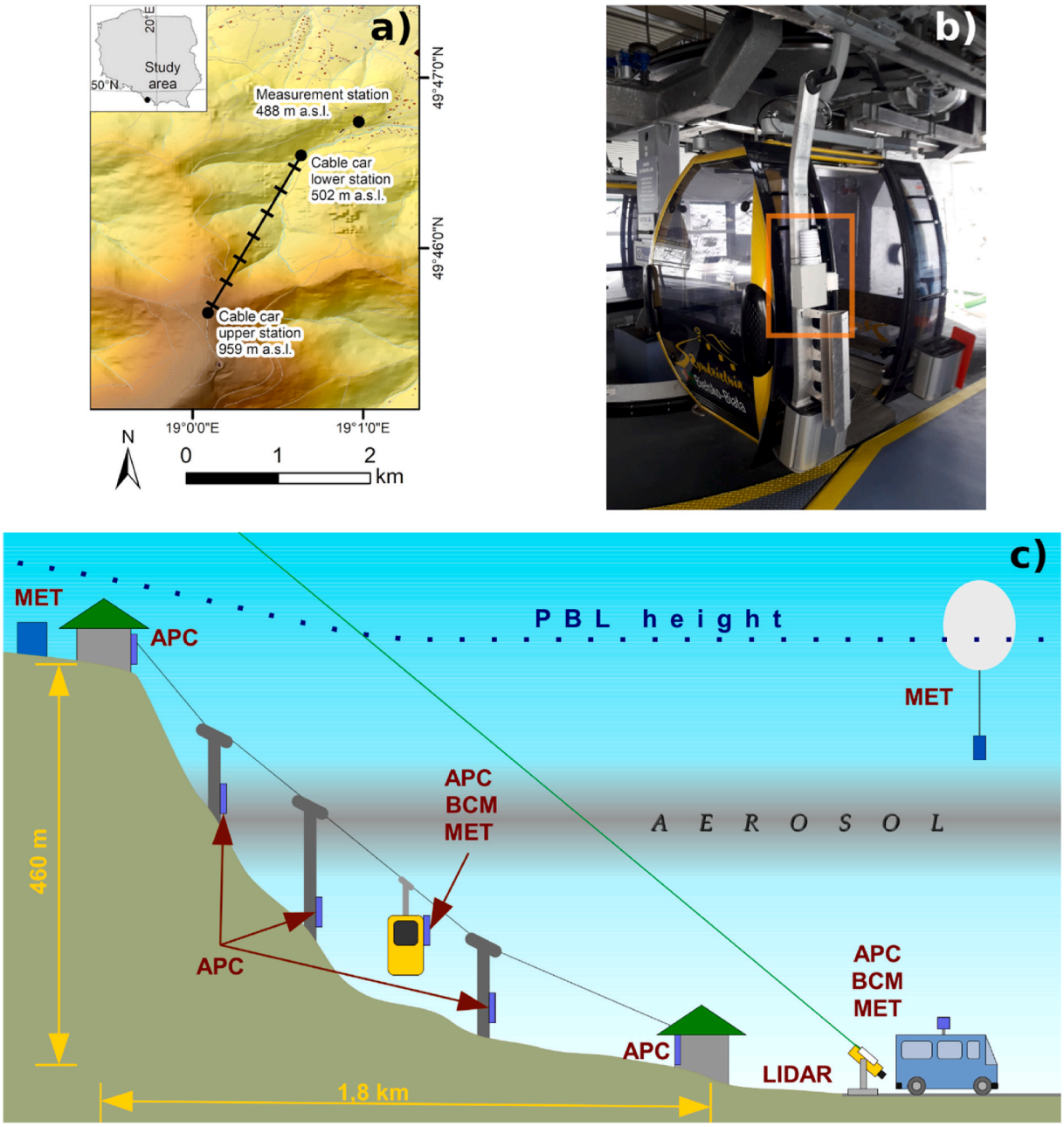

Fig. 1. Illustration of (a) the research area, (b) the mobile platform for aerosol profiling on a cable car, and (c) the scheme of the measurement site. Distance between the two cable car measurement sites (lower and upper) is approximately 1.8 km in the horizontal and approximately 460 m in the vertical direction. Travel time of the cable car was approximately 9 min. PBL-planetary boundary layer, APC-aerosol particle counter, BCM-black carbon concentration meter, and MET-measurements of meteorological conditions (temperature, humidity, pressure, and wind). The box with aerosol equipment including optical particle counters (PMS7003 and OPC-N2), a micro-aethalometer (AE-51), air temperature, relative humidity, air pressure sensors (HTU21, BME280), a global positioning system (GPS) receiver, and an internal power supply was placed on a bicycle holder on the side door of a cable car (orange frame). (For interpretation of the references to colour in this figure legend, the reader is referred to the Web version of this article.)

sensing techniques and in situ methods using various atmospheric probing platforms (Devara, 1998). Remote sensing techniques are based on sun photometers or lidars. Sun photometers allow the determination of the columnar properties of aerosols, such as optical depth and single scattering albedo (SSA), while lidars provide vertical profiles of the optical properties of the aerosol, such as backscatter and extinction coefficients. Lidar measurements provide information with high time resolution in the order of seconds or minutes, and a spatial resolution in the order of several meters. The main limitation of lidars in smog profiling is geometric compression. This makes it possible to determine the optical parameters of aerosols only from a certain height (Stelmaszczyk et al., 2005). An alternative to lidars are ceilometers. Although they are dedicated to cloud base detection, they can be used to measure aerosols, at least in the boundary layer of the atmosphere (Markowicz et al., 2008). Some ceilometers have low geometric compression, meaning that aerosols can be detected as low as several meters above the ground.

For in situ smog profiling, instruments are placed on unmanned aerial vehicles (UAV) (Bates et al., 2013; Chilinski et al., 2018), tethered balloons (Ferrero et al., 2014; Hara et al., 2013), or cable cars (Zawadzka et al., 2017). In these cases, miniature equipment measures the concentration of particulate matter (PM), especially $PM_{2.5}$ and PM_{10},

and the equivalent black carbon (eBC) concentration. Research conducted by Chilinski et al. (2016, 2018) in an aerosol background station area in southeastern Poland and in the region of the Warsaw agglomeration showed that a UAV-based system was able to measure smog profiles in the lower troposphere. However, ceilometers (CHM15k and CL31) were unable to register the accumulation of pollutants in the vicinity of the earth's surface. Observed aerosol concentration changes in the first few dozen meters reached two orders of magnitude. In particular, large gradients of both aerosol concentration and meteorological parameters were recorded at the upper inversion limit in a layer of a few meters thick.

Measuring equipment can also be carried by tethered balloons; they are used for research worldwide (e.g. Ferrero et al., 2014; Markowicz et al., 2017). However, in the case of drones and tethered balloons, the main limitations involve airspace availability, for example, questionable areas, such as the vicinity of airports, and other factors including wind direction and speed. For tethered balloons, the wind speed should not exceed a few meters per second (approximately 5 m/s), whereas for drones, this limit is approximately 10 m/s. Markowicz et al. (2017) and Chilinski et al. (2019) combined data obtained from UAVs and tethered balloons with lidar and ceilometer measurements to determine additional optical properties of the aerosols, such as the SSA profile or the absorption optical depth. These values are the basic atmospheric parameters necessary to simulate solar radiation fluxes as well as aerosol radiative forcing.

Another type of measurement platform used for atmospheric measurements are cable cars. This type of platform has some limitations, for example, profiling can only be performed on the cable car route, and it is quasi-vertical profiling because a cable car moves vertically and horizontally. The main advantage of using a cable car is the long operation time, for example, 8 h, which is difficult for most of drones. However, the duration of the measurements is limited to the cable car's opening hours. Instruments mounted on cable cars can profile the atmosphere in restricted areas, such as national parks where UAVs cannot operate. Using a cable car is also less costly and simpler to operate than a UAV or a tethered balloon. Measurements on the cable car are also less dependent on weather conditions. The miniaturisation of measurement equipment (Markowicz and Chilinski, 2020; Pang et al., 2021) makes cable car measurements more popular in atmospheric sciences, such as climatology (Seidel et al., 2016) and aerosol profiling (Duan et al., 2021; Zawadzka et al., 2017), particularly black carbon (BC) exposure (Madueño et al., 2020).

In Krynica in 2016 (Lesser Poland Voivodeship), Zawadzka et al. (2017) tested the possibility of placing the equipment for measuring properties of aerosols on a |Mt. Jaworzyna Krynicka cable car. The micro-aethalometer and optical particle counter were mounted on the cable car and used to measure the profiles of eBC concentration and aerosol size distribution. During the campaign, a significant correlation was found between the temperature gradient and the difference in the extinction coefficient between the valley and the mountain. The profiles obtained from cable car measurements showed a significant reduction in eBC and aerosol concentration with altitude. The results of these studies were very promising, and in 2018, a three-week research experiment was organised in the Mt. Szyndzielnia area (the Silesian Beskids). Smog in Bielsko-Biala (southern Poland) during the winter season was examined. The main objective of this study is to understand the vertical variability of aerosol optical and microphysical properties under different meteorological conditions.

2. Field experiment and equipment

2.1. Strategy of measurements

The measurement campaign was conducted from 25 February to March 11, 2018 in Bielsko-Biala, a city in southern Poland in Silesian Voivodeship. The topography of the study area is diverse and includes both upland and mountain areas. The centre of Bielsko-Biala lies at an altitude of 313 m a.s.l. The highland part of Bielsko-Biala consists of several hills, separated by valleys with rivers and streams. The three highest peaks of the Silesian Beskid are located within the administrative borders of Bielsko-Biala, including Szyndzielnia (1030 m a.s.l.).

Central heating systems have the greatest impact on air pollution in the Bielsko-Biala area. The household sector and small and medium sized enterprises burn coal for heating or technological purposes. The inhabitants of the downtown area of Bielsko-Biala still use traditional solutions with individual coal and coke boilers. This contributes to increasing air pollution in the area.

The measuring equipment was placed in several locations near the Szyndzielnia cable car (Fig. 1a). The lower measuring station (LMS) included two locations approximately 500 m apart. One was a mobile laboratory in a van parked at 490 m a.s.l. (49.7790 N, 19.0166 E) and the other was a platform of the lower station of the Szyndzielnia cable car at 502 m a.s.l. (49.7755 N, 19.0107 E). A set of sensors was installed on three cable car supports on the slope of Szyndzielnia at 621, 726, and 878 m a.s.l., respectively (Fig. 1c).

The upper measuring station (UMS) was in the area of the upper cable car station (49.7603 N, 19.0018 E) at an altitude of approximately 960 m a.s.l. (Fig. 1c), the relative height between the lower and the upper cable car station was approximately 460 m, and the straight-line distance was 1749 m. The time of the one-way ride ranged from 6 to 12 min depending on the cable car speed. This allowed for relatively rapid atmospheric profiling using the cable car as a platform for the measuring equipment.

2.2. Equipment

The measurements included thermodynamic air parameters, such as temperature, humidity, total aerosol concentration, and eBC concentration. The aerosol optical properties were measured using in situ and remote sensing techniques.

The meteorological parameters were measured using the following instruments. A meteorological station (Vaisala 520XT) was installed in the LMS. Areological soundings with Vaisala RS92SGP radiosondes were also conducted from the LMS. A meteorological station (Davis Vantage Pro2) was installed in the UMS.

The aerosol-related measurements were performed using the following instruments: at the LMS, a multiwavelength lidar, an AE-31 aethalometer (Magee Scientific), a photoacoustic extinctiometer (PAX 532 nm and PAX 870 nm), PMS7003 (Plantower), and OPC-N2 (Alphasense) particle counters were used. At the UMS, a set of PMS7003 and OPC-N2 particle counters was used. Aerosol device inlets were mounted approximately 3 m above ground level. Aerosol sensors (PMS7003) were fixed 2 m above ground level on three cable car supports on the slope of Szyndzielnia.

The set for profiling on the cable car consisted of air temperature, relative humidity, and air pressure sensors (HTU21, BME280), PMS7003 and OPC-N2 optical particle counters, an AE-51 micro-aethalometer, and a GPS receiver. A box with aerosol equipment and an internal power supply was placed on a bicycle holder on the side door of the cable car (Fig. 1b).

In situ measurements of the optical properties of aerosols were taken using an AE-31 aethalometer and photoacoustic devices. An aethalometer measures, in real time, the attenuation of a light beam transmitted through a filter, on which suspended PM is collected. Aerosol particles were deposited on a tape made of quartz refractory fibres 1 μm in diameter and cellulose fibres 10 μm in diameter. The main part of the instrument was an optical head equipped with one or more optical channels. A light beam passes through the filter, and therefore, weakens. The light absorption coefficient and the concentration of eBC were determined on that basis. The main limitations of this method were the light multi-scattering and aerosol loading artifacts. Compensating for these effects is difficult and can be done if the aethalometer

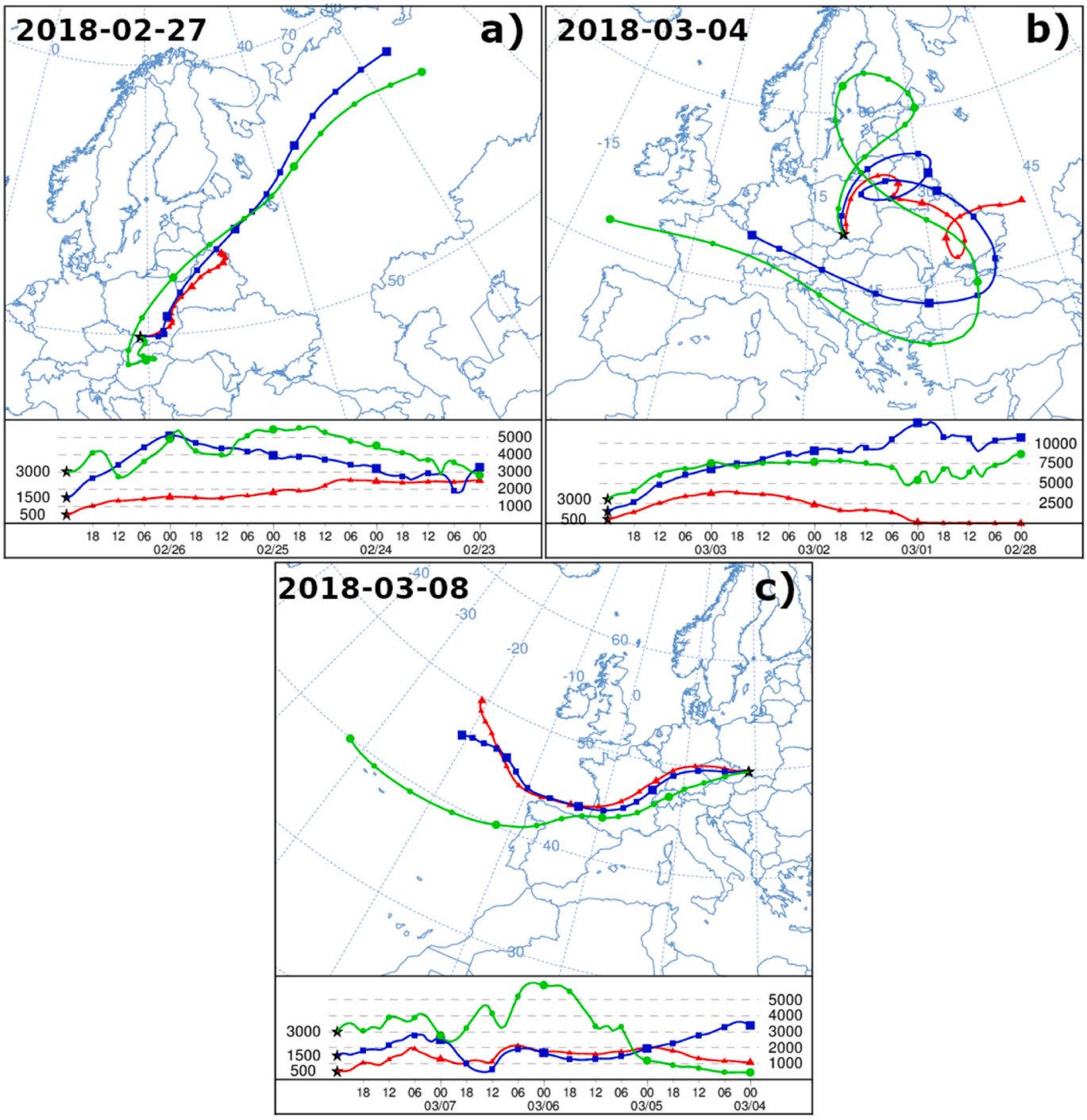

Fig. 2. Hybrid single particle Lagrangian integrated Trajectory model (HYSPLIT) back-trajectories obtained for Bielsko-Biala typical for (a) 25–28 Feb 2018, (b) 01–06 Mar 2018, and (c) 07–10 Mar 2018. The HYSPLIT model was run for 96 h with meteorological data from the Global Data Assimilation System (GDAS).

measurements are taken simultaneously with the scattering coefficient measurement, for example, by a nephelometer (Collaud et al., 2010). Two aethalometers were used in this study, namely, a stationary AE-31 (Hansen et al., 1984) and a portable microAeth AE-51 placed on the cable car (Cheng and Lin, 2013).

Another measurement technique in which the effects of light scattering do not occur is the photoacoustic method (Nakayama et al., 2015). The two-wavelength (532 and 870 nm) photoacoustic extinctiometer (PAX, Droplet Measurement Technologies) measures aerosol single-scattering properties such as scattering and absorption coefficient, SSA, and eBC mass concentration (Kok et al., 2010). The photoacoustic method has become a standard technique for measuring the absorption of radiation by atmospheric aerosols. The PAX detects pressure waves initiated by the emission of energy from the absorbing particles and, therefore, estimates the level of absorption. Its main element is the photoacoustic chamber where the laser is located. The construction of the scattering chamber is based on the nephelometer technique. The detector measures the scattering light between 6° and 174°.

Aerosol size distributions were determined using PMS7003 and OPC-N2 miniature particle counters. The measurement techniques for both instruments were similar. The particles pass through the measuring

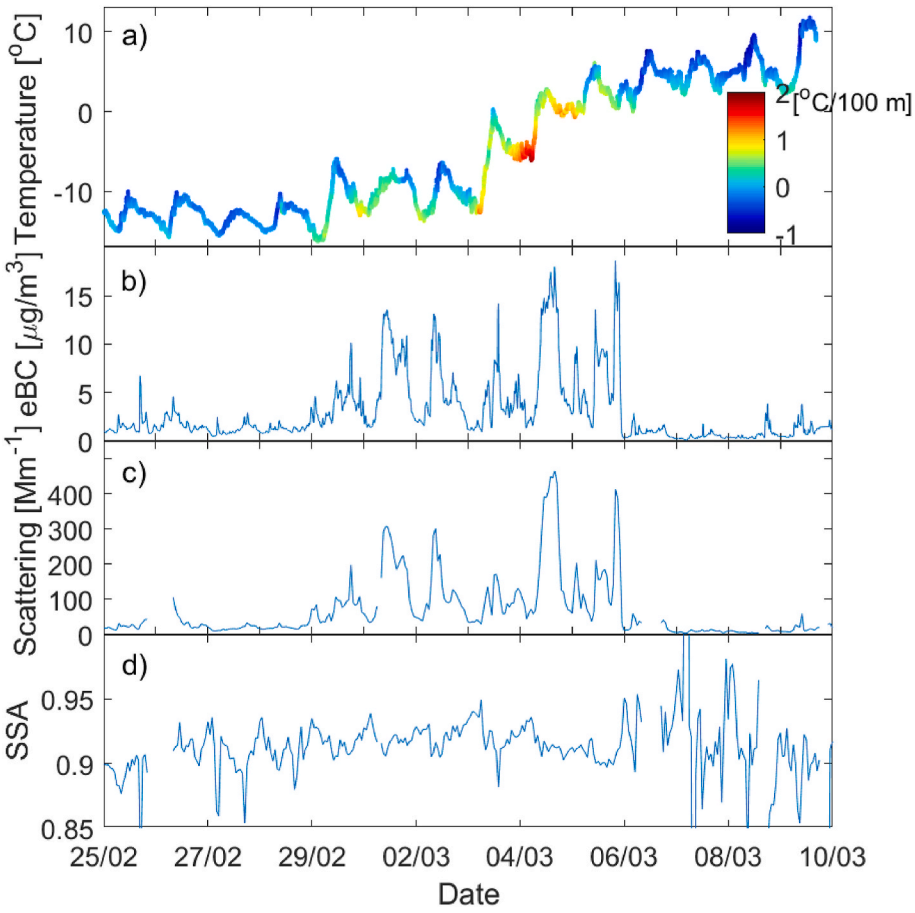

Fig. 3. Temporal variability of (a) air temperature at LMS in °C, (b) eBC concentration from AE-31 in μg/m^3, (c) aerosol scattering coefficient in Mm^{-1}, and (c) single scattering albedo at 870 nm from PAX devices. The coloured line in panel (a) shows air temperature gradient in [°C/100 m] obtained from the temperature difference between the LMS and UMS stations. Warm colours correspond to inversion conditions (temperature gradient above 1 °C/100 m), yellow, green, and light blue colours coincide with isotherms and slight inversion, and blue colours correspond to conditions with a negative temperature gradient. (For interpretation of the references to colour in this figure legend, the reader is referred to the Web version of this article.)

chamber, a laser diode emits a beam, and the light scatters on the particles. The intensity of the scattered light enabled the estimation of the particle sizes. As a result, the instruments reported the concentration of the particles in 16 (OPC–N2) and 5 (PMS7003) bin sizes and the mass concentrations of PM_1, $PM_{2.5}$, and PM_{10} (Bulot et al., 2019).

Remote measurements were taken using a Microtops hand-held sun photometer (Morys et al., 2001), which was used to measure the direct flux of solar radiation reaching the Earth's surface. The sun photometer was equipped with five spectral channels, with wavelengths of 380, 500, 675, 870, and 1020 nm, and a half-width of 10 nm. Atmospheric aerosol profiling using a hand-held sun photometer is limited to relevant meteorological conditions. During the measurement, the solar disk cannot be obscured by clouds, which significantly limits the possibility of taking measurements in the autumn and winter periods.

A prototype 3-wavelength lidar developed at the Faculty of Physics, the University of Warsaw was used to determine the PBL height and aerosol layers (Posyniak et al., 2010, 2011). A pulsed Nd:YAG laser (Brilliant, Quantel) was mounted in this device setup in the optical transmitter. The laser generated light pulses at wavelengths of 1064 nm, 532 nm, and 355 nm, with energies of 100 mJ, 60 mJ, and 40 mJ, respectively. The duration of the pulses was 6 ns, and the repetition rate was 10 Hz. In the optical receiver, a Cassegrain telescope with a mirror 150 mm in diameter was used. The return light pulses collected by the telescope were spectrally separated by a polychromator and registered in the channels corresponding to the consecutive wavelengths. The signals from the photomultipliers installed in each channel were digitised by 12-bit, 50 MHz A/D converters (Tie Pie Handyscope HS4). To increase the signal-to-noise ratio, the data were averaged over 90 s time intervals and then smoothed over the altitude intervals of 30 m. The lidar overlap distance reached an altitude of approximately 150 m (Stelmaszczyk et al., 2005). To investigate the aerosol at low altitudes, starting from 75 m, the laser beam was sent towards an angle of 30° to the horizontal plane. Unfortunately, due to laser failure, only one channel of the lidar (1064 nm) laser was functional during the measurement campaign, and aerosol size distributions could not be derived.

2.3. Calibration of instruments

Low-cost aerosol counters (PMS7003) were calibrated against the GRIMM EDM 180 (Environmental Dust Monitor) at the Swider station in central Poland immediately after the field campaign. The calibration duration was three weeks, and after that time the results of the PMS and the GRIMM measurements were compared. The comparison data were in good agreement, but it was found that PMS values were too high (Fig. S1). Therefore, the linear regression coefficients were calculated to correct the PM_{10} mass concentration from the PMS instruments.

The Microtops sun photometer is calibrated every year within the Poland-AOD network (Markowicz et al., 2016). The PAX devices were calibrated by the manufacturer in 2016.

3. Temporal changes of aerosol optical parameters in the context of meteorological conditions

This section presents a short analysis of the temporal changes in meteorological and aerosol conditions during the experiment at an LMS. Large changes in the extensive aerosol optical properties, that is, light scattering coefficient related to the development and disappearance of the smog conditions, characterise the analysis period.

The analysis period was divided into three phases according to the type of atmospheric circulation (Fig. 2). These conditions influenced the temperature inversions and consequently, the aerosol concentration.

In the first phase of the study on 25–28 February 2018, the extensive

Table 1
Mean and standard deviation values of meteorological and aerosol optical parameters during three periods of field campaigns measured at the lower station (502 m a.s.l).

	1st period 25–28.02.2018	2nd period 1–6.03.2018	3rd period 7–11.03.2018
Temperature [°C]	−13.1 ± 1.2	−6.0 ± 5,7	5.2 ± 2.3
Temperature gradient [°C/100 m]	−0.7 ± 0.2	−0.1 ± 0.5	−0.7 ± 0.3
Relative humidity [%]	71.8 ± 6.3	65.0 ± 10.5	63.9 ± 10.7
eBC concentration [μg/m^3]	1.45 ± 0.88	5.39 ± 4.42	0.90 ± 0.95
Absorption Angstrom exponent	1.62 ± 0.07	1.61 ± 0.09	1.68 ± 0.19
Absorption coefficient at 532 nm [Mm^{-1}]	8.7 ± 4.3	31.6 ± 20.7	8.8 ± 9.9
Scattering coefficient at 532 nm [Mm^{-1}]	70.6 ± 25.6	338.9 ± 250.0	73.7 ± 40.24
Extinction coefficient at 532 nm [Mm^{-1}]	79.3 ± 27.0	370.5 ± 269.5	82.5 ± 43.0
Single scattering albedo at 532 nm	0.89 ± 0.05	0.91 ± 0.03	0.89 ± 0.04
Absorption coefficient at 870 nm [Mm^{-1}]	2.4 ± 2.5	12.0 ± 10.5	1.4 ± 2.26
Scattering coefficient at 870 nm [Mm^{-1}]	24.3 ± 13.9	130.1 ± 104.7	14.1 ± 11.8
Extinction coefficient at 870 nm [Mm^{-1}]	26.7 ± 15.1	142.1 ± 115.1	15.5 ± 13.4
Single scattering albedo at 870 nm	0.90 ± 0.03	0.92 ± 0.02	0.92 ± 0.05
Angstrom exponent	1.98 ± 0.42	1.77 ± 0.76	3.2 ± 0.69

Omega high-pressure system from the Gulf of Bothnia shaped the meteorological conditions. Poland was in a zone of influence of cold polar continental air. The backward trajectories of the air masses from HYSPLIT (Stein et al., 2015) indicate that a frosty mass of air flowed into Poland from the Barents Sea, Franz Josef Land, Novaya Zemlya, and northwestern Siberia (Fig. 2a).

In the first days of the experiment, the air temperature was low and below −5 °C all day. During the night, it dropped to below −15 °C. On 3 March, there was significant warming that systematically progressed towards the end of the study period.

The air inflow was variable. On 27 February, air flowed over Poland between 500 and 3000 m from the north-eastern direction (Belarus and Russia) and started to push the polar sea air at higher altitudes. On 1 March, a cyclonic system began to form over the Azores region, moving from Spain toward Great Britain, and over Germany; it brought significantly warmer polar sea air. On 2 March, a low-pressure centre was created over Ukraine, causing the exchange of air masses in Poland. Over the following days, the warming was associated with the influx of a warm polar sea mass from the Bay of Biscay, where a low-pressure centre was formed. The change in the direction of the air inflow to the west is clearly visible on the retrograde trajectories (Fig. 2b). From 7 to 10 March in southern Poland, including the study area, the foehn effect occurred, bringing warm and dry air from above the mountains. Backward trajectories at levels from 500 to 3000 m indicate a strong zonal flow (Fig. 2c) of the polar sea air mass.

Fig. 3a indicates the changes in the air temperature and the temperature gradient between the upper and lower stations at altitudes of 960 and 502 m above sea level, respectively.

In the middle phase of the study from 1 to 6 March 2018, significant temperature inversions were observed, which persisted during the day on 5–6 March 2018. During the inversion period, the extensive parameters describing the amount of aerosol in the air increased significantly. The concentration of eBC (Fig. 3b) exceeded 15 μg/m^3 several times. The two-week campaign period was divided into three periods with different atmospheric parameter values (Table 1). These were 25–28 February, 1–6 March, and 7–11 March. In the period from 1 to 6 March,

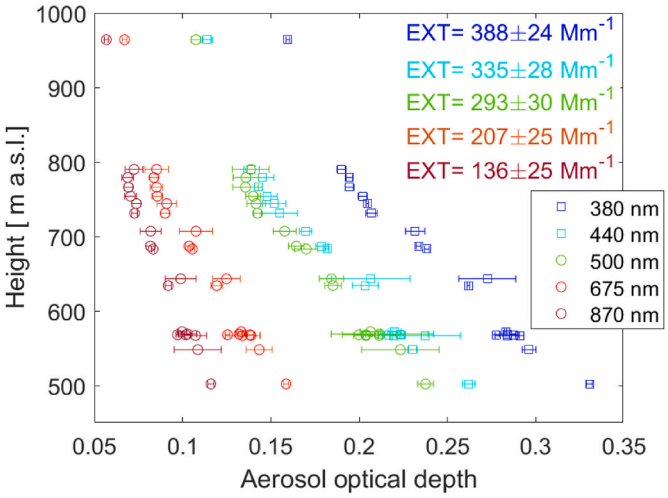

Fig. 4. Vertical profile of aerosol optical depth obtained on March 4, 2018 using a Microtops sun photometer at 11:30–11:45 UTC. Navy blue, blue, green, red, and brown colours correspond to 380 nm, 440 nm, 500 nm, 675 nm, and 870 nm, respectively. The horizontal lines indicate the measurement uncertainty related to the imprecise orientation of the instrument towards the sun disk. (For interpretation of the references to colour in this figure legend, the reader is referred to the Web version of this article.)

the mean and standard deviation level of eBC was 5.39 ± 4.42 μg/m^3; in the first and third phase, the values were 1.45 ± 0.88 μg/m^3 and 0.90 ± 0.95 μg/m^3. The aerosol conditions measured in the first and third phases were at the background aerosol level. Juda-Rezler et al. (2016) reported the mean values of eBC in the background station (SolarAOT) in southeastern Poland in February and March at the level of 2.0 μg/m^3 and 1.5 μg/m^3, respectively. Therefore, average values below 1.5 μg/m^3 should be treated as low, particularly because they refer to values measured in urban conditions. The light scattering coefficient (Fig. 3c), analogous to the eBC concentration, was 4–5 times higher in the middle phase than at the beginning and the end of the study period. Only SSA did not change significantly during the study period. This parameter indicates the contribution of scattering processes to the total radiation extinction. A value of approximately 0.9 (Fig. 3d) indicates a significant proportion of absorbing aerosol. The lack of large variations in this size implies a relatively constant contamination of absorbing particles, mainly soot, which indicates slight changes in the intensity of various types of emissions.

Although the average air temperature in the first phase of the experiment was 18 °C lower than in the third phase, the physical parameters of the aerosol were only slightly lower. This may be explained by the atmospheric conditions that did not develop the near-ground temperature inversion during this period. The average daily temperature gradient in the first and third phases was close to the average temperature gradient in the troposphere and equal to −0.7 °C/100 m.

4. Analysis of vertical profiles

4.1. Sun photometer profiles

As part of the study, profiling was performed with the Microtops sun photometer during the cable car ride on March 4, 2018 from 11:30 to 11:45 UTC. Measurements were taken through the open window of the cable car by manually pointing the device towards the sun disk. Fig. 4 shows the aerosol optical depth (AOD) profiles for the wavelength. This value in every case decreased with height because of the decrease in the column of air mass above the device. Changes in AOD with height were greater in the lower layer than below the top of Szyndzielnia. In the air layer approximately 150 m below the summit, there is no data because

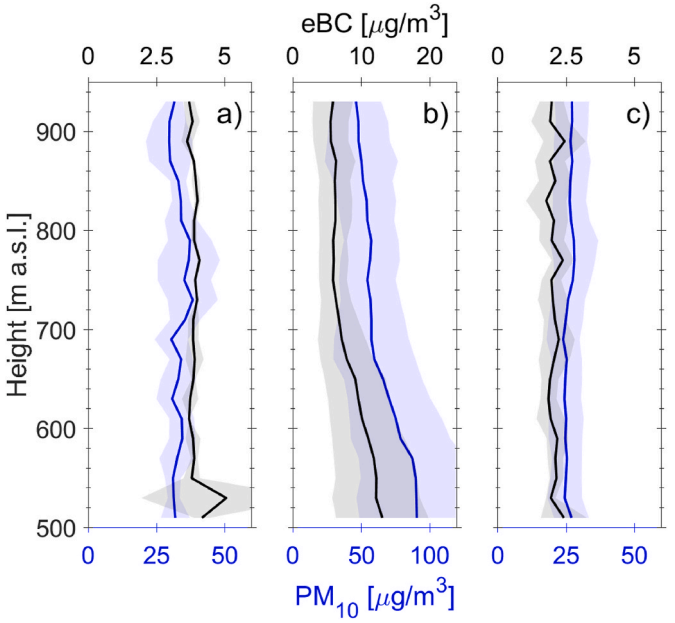

Fig. 5. Mean vertical profiles of PM_{10} in [μg/m^3] (blue line) and eBC concentration in [μg/m^3] (black line) from cable car measurements obtained in the morning hours (before 10 UTC). On (a) February 28, 2018, (b) between 1 and March 6, 2018, and between (c) 7 and March 10, 2018. Shading corresponds to standard deviation of the profiles. Note that the scale of the x-axis is different for different stages of the experiment. (For interpretation of the references to colour in this figure legend, the reader is referred to the Web version of this article.)

the car was moving in the shade of the surrounding trees. The change in AOD between the lower and upper stations varied from 42 to 49%, depending on the wavelength. This showed a very heavily polluted layer of the atmosphere that was almost 500 m thick, in which almost half of aerosols, in the optical sense, were present.

The average aerosol extinction coefficient between the lower and upper stations of the cable car was determined based on the changes in the AOD (Fig. 4). This value varied from 136 to 388 Mm^{-1} between 380 and 870 nm. For comparison, the extinction coefficient measured at LMS by the PAX device was 314 ± 31 Mm^{-1} at 532 nm, and the SSA was 0.91 ± 0.01, while at 870 nm it was 138 ± 11 and 0.92 ± 0.01, respectively. Notably, the measurements taken in the LMS using the PAX devices were performed in dry conditions (relative humidity of 39%), while the estimated extinction coefficient based on the data from the sun photometer was in ambient conditions. During measurements with a sun photometer, the relative humidity in the upper and lower stations was 54% and 35%, respectively. In this case, it is expected that the hygroscopic growth effect is small because the relative humidity is low at both LMS and UMS (Zieger et al., 2013). Therefore, the extinction coefficients measured by the different methods were similar.

4.2. Aerosol profiles from the cable car

This section presents the results of the lower troposphere profiling on the slopes of Szyndzielnia. To obtain the vertical profiles of PM_{10} and eBC mass concentration, the data were averaged in 20 m thick layers from 500 m a.s.l. up to 960 m a.s.l. In the case of the AE-51 data, the optimised noise reduction averaging (Hagler et al., 2011) method was used. Fig. 5 presents the mean vertical profiles of PM_{10} and eBC mass concentrations obtained in three periods of the experiment in the morning hours before 10 UTC. The mean PM_{10} and eBC profiles for the first and third periods show small variability with altitude (Fig. 5a and c, respectively). A significant change is observed in the second stage (Fig. 5b). PM_{10} decreased from approximately 90 μg/m^3 close to the surface to 50 μg/m^3 (upper station). The reduction in eBC was from approximately 12 μg/m^3 to 6 μg/m^3. For both PM_{10} and eBC, the reduction was mostly observed in the first 150–200 m. In the upper layer, both quantities changed slightly. The significant reduction in aerosol mass concentration with altitude can be explained by surface or lower troposphere temperature inversions, which were observed every

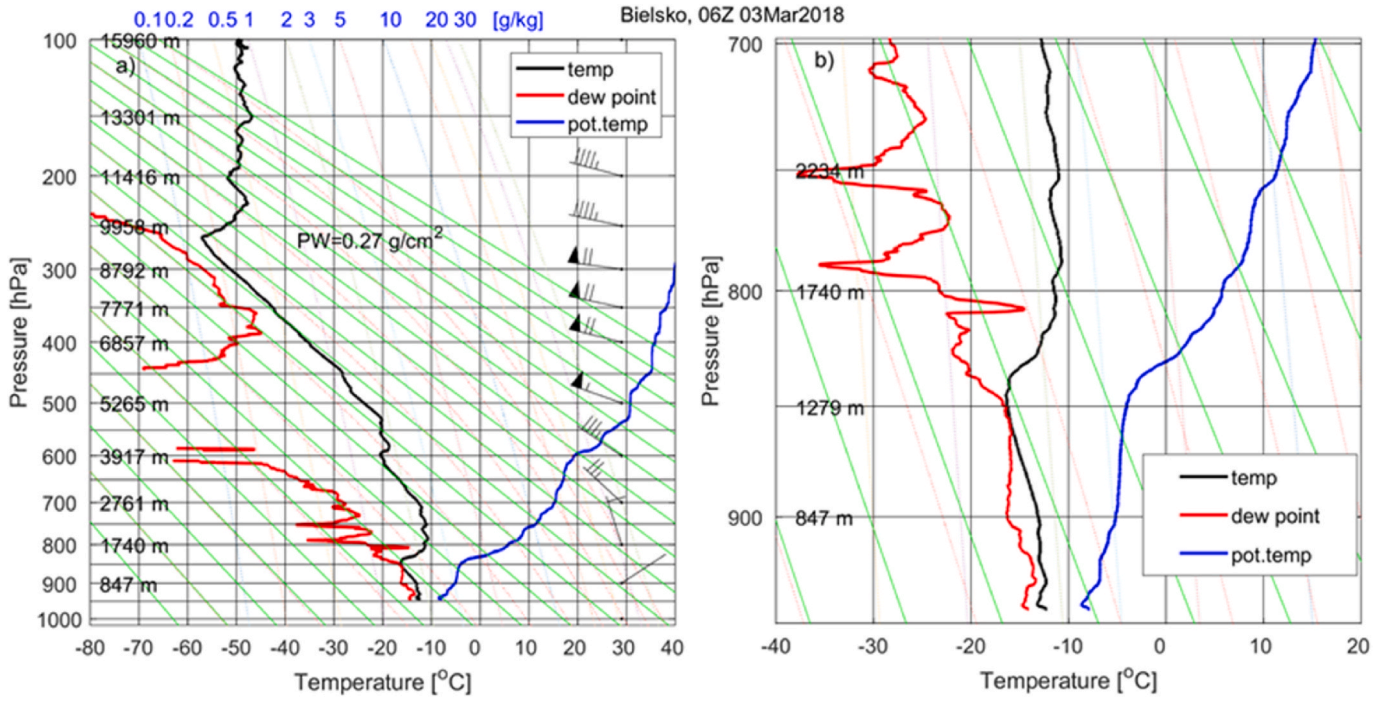

Fig. 6. Stüve diagram obtained on March 3, 2018 at 06 UTC from RS92SGP radiosonde profile. Black, red, and blue lines show air temperature, dew point, and potential temperature, respectively. Panel (b) shows the enlarged view of the lowest troposphere (upper level of 700 hPa). (For interpretation of the references to colour in this figure legend, the reader is referred to the Web version of this article.)

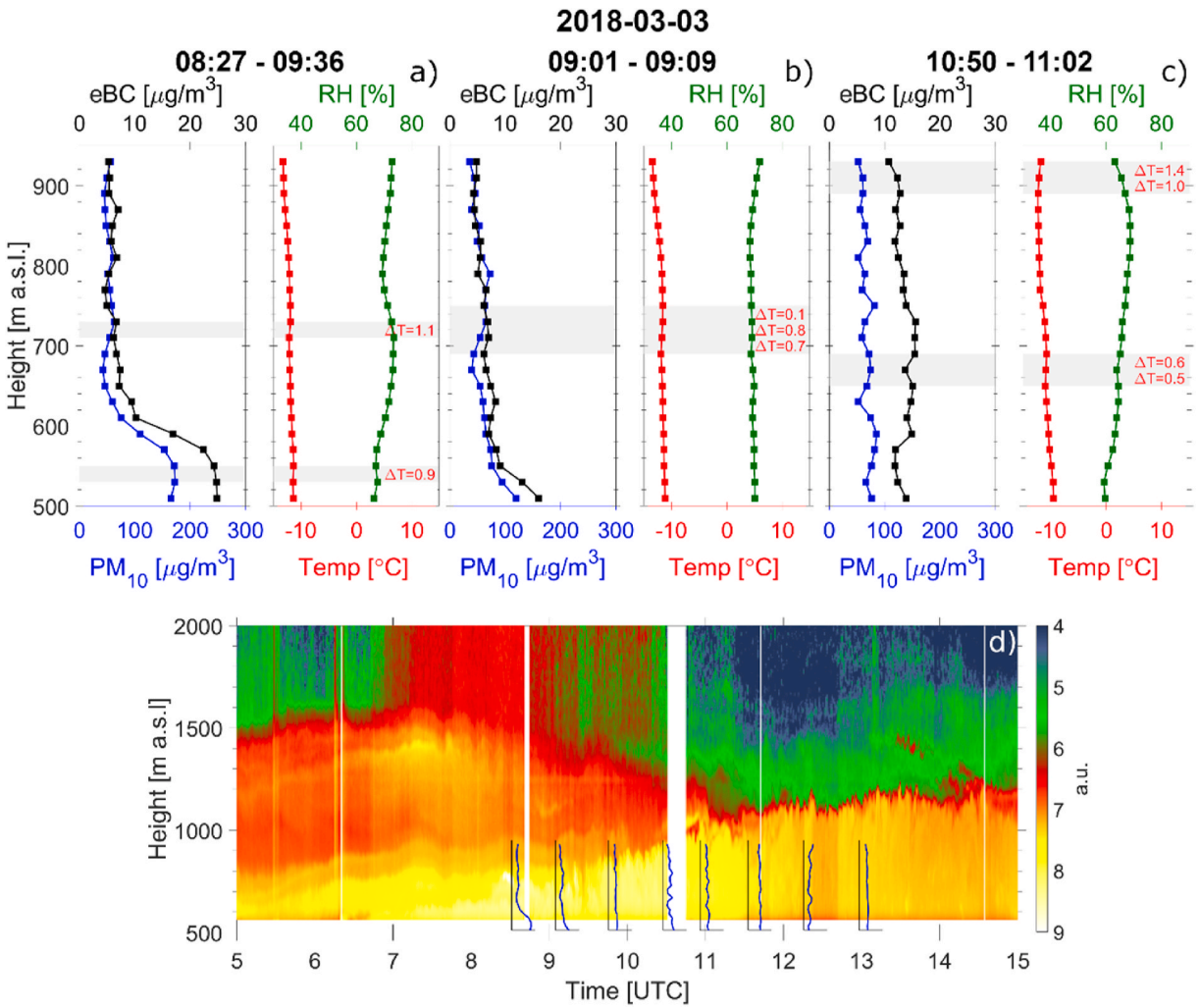

Fig. 7. Vertical profiles of PM_{10} in [μg/m^3] (blue line), eBC concentration in [μg/m^3] (black line), air temperature in [°C] (red line), and relative humidity in [%] obtained during cable car soundings on March 3, 2018 between (a) 08:27–08:36 UTC, (b) 09:01–09:09 UTC, and (c) 10:50–11:02 UTC. Grey shadows indicate inversion layers. Logarithm of range-corrected lidar signal (at 1064 nm) registered on March 3, 2018 (d). Additional blue lines correspond to PM_{10} mass concentration profiles. (For interpretation of the references to colour in this figure legend, the reader is referred to the Web version of this article.)

night during the second stage of the field campaign (Fig. 3a).

The results of the profiling of the slopes of Szyndzielnia on 3 and March 5, 2018 are presented as follows: Before the cable car was put into operation, aerological sounding was performed at 06 UTC. On 3 March there was a temperature isotherm in the ground layer (up to 850 m a.s.l.) and a strong subsidence inversion (approximately 7 °C) from a height of approximately 1.5 km. Another isothermal layer was observed between 1.5 and 1.7 km and 4.0 and 5.0 km, where a very low dew point temperature (below −65 °C) was recorded. The monotonic rise of potential temperature changes with height indicates stable thermodynamic conditions in the lower troposphere and poor vertical air mixing (Fig. 6).

Fig. 7 shows the thermodynamic and aerosol concentration profiles obtained on 3 March during three rides of the cable car starting at (a) 08:27 UTC, (b) 09:01 UTC, and (c) 10:50 UTC. The eBC and PM_{10} mass concentration profiles show maximum values in the first 60–70 m of the atmosphere (eBC at the level of 20 μg/m^3 and PM_{10} at approximately 180 μg/m^3). In this layer, a slight temperature inversion was observed (0.9 °C/100 m). Above this layer, aerosol concentrations dropped significantly and were below 10 μg/m^3 for eBC and below 100 μg/m^3 for PM_{10}. The concentration profile from 600 m a.s.l. to the summit of Szyndzielnia shows slight fluctuations. At a height of approximately 200 m above the lower station, a slight temperature inversion is visible, with a slight rise in PM_{10}. In the case of the second profile made half an hour later, visible changes are only observed in the ground layer. The eBC and PM_{10} values decreased to approximately 15 μg/m^3 and 120 μg/m^3, respectively. The ground-level inversion disappears in the thermodynamic profile, while the inversion at 700–750 m a.s.l. is widened without changing the aerosol concentration. The last of the presented profiles from that day was made at approximately 11 UTC. Concentrations of PM_{10} and eBC do not show large changes with height during this time, which indicates intensive mixing processes. Inversion below 700 m remains present, and a new inversion layer is visible just below the top of the Szyndzielnia peak.

Fig. 7d shows the logarithm of the lidar range-corrected signal and vertical profiles of PM_{10} and mass concentration from cable car soundings. Lidar data show variability in the aerosol surface layer (below the green thin layer) from approximately 1500–1600 m a.s.l (morning) to 1100–1200 m a.s.l (afternoon). In the lidar data, there is some evidence of an increase in PBL height from 5 to 6 UTC until 11–12 UTC. The maximum signal close to the surface, detected by cable car profiling, is not observed in the lidar data, probably due to overlap problems in the first 40–50 m.

The meteorological sounding conducted at 06 UTC on 5 March, just before the cable car profiling, shows a stable thermodynamic condition of the air mass and approximately twice as much water vapour than two days earlier. The ground inversion is approximately 4.5 °C and reaches

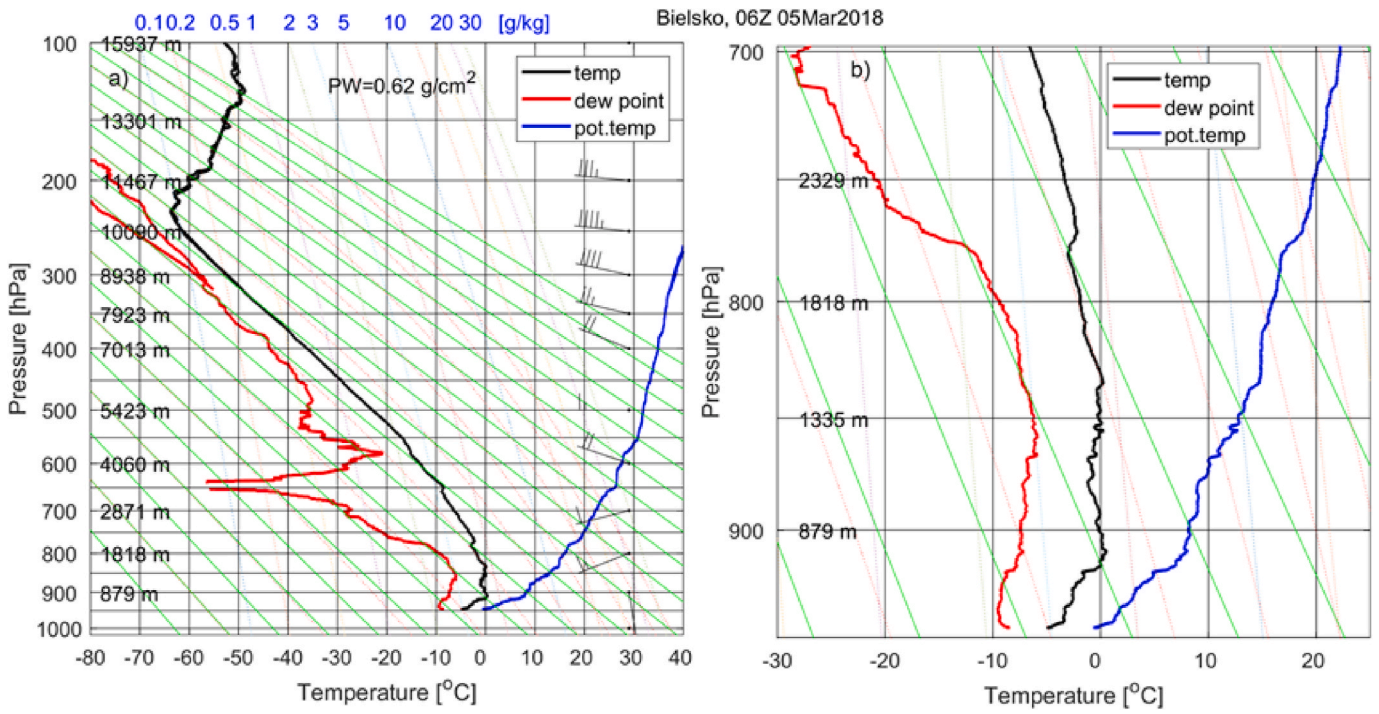

Fig. 8. Stüve diagram obtained on March 5, 2018 at 06 UTC from the RS92SGP radiosonde profile. Black, red, and blue lines indicate air temperature, dew point, and potential temperature, respectively. Panel (b) shows the enlarged view of the lowest troposphere (upper level of 700 hPa). (For interpretation of the references to colour in this figure legend, the reader is referred to the Web version of this article.)

800 m a.s.l. Above, in a layer approximately 1 km thick, the air temperature changes very little. At an altitude of approximately 3.5 km, a slight subsidence inversion is visible, above which the dew point temperature drops significantly (Fig. 8).

Fig. 9 demonstrates the thermodynamic profiles and concentrations of eBC and PM_{10} during the three rides of the cable car on 5 March. Compared with the conditions on 3 March, the air layer between the lower and upper stations of the cable car is within the range of a significantly higher inversion, which remained above the ground even during the midday hours. Despite this, the mass concentration values of eBC and PM_{10} are not significantly higher than those of two days earlier.

The eBC values in the first profile reach 10 μg/m^3 at the ground surface and approximately 5 μg/m^3 at the height of the upper station on Szyndzielnia. The value of eBC at the level of 5 μg/m^3 near the upper station should be treated as very high and probably several times higher than the average for this period. Like eBC, vertical changes in PM_{10} are not significantly high. However, the mass concentration of particles in the entire layer is high, being from 120 μg/m^3 at the ground surface to approximately 70 μg/m^3 at 650 m a.s.l., and 80 μg/m^3 at the height of Szyndzielnia. Vertical changes in eBC and PM_{10} in the second profile are significantly greater. There is a visible increase in the mass concentration at the ground surface to 20 μg/m^3 for eBC, and 170 μg/m^3 for PM_{10}. The third profile shows no changes in eBC with height; however, the measured values are very high at approximately 20 μg/m^3. In the case of PM_{10}, the values fluctuate around 200 μg/m^3 and drop below 100 μg/m^3 just below the upper station. The high values of aerosol mass concentration around the upper station indicate slow (poorly effective) vertical mixing above the top, which results in an entrapment of the particles in the first several hundred metres. The results from aerosol profiling indicate an approximately 10% share of eBC in the mass of particles below 10 μm. The aerosol layer in the lidar data (Fig. 9d) is thinner than on 3 March. The top of the aerosol layer is approximately 1000 m a.s.l. in the morning to 1200–1300 m a.s.l. in the afternoon. The increase in the logarithm of the range-corrected signal close to the surface since 8 UTC is consistent with the increase in PM_{10} mass concentration.

5. Summary

The results of the field experiment conducted on the slopes of Szyndzielnia at the turn of February and March 2018 were presented. An innovative method for quasi-vertical profiling of the optical and microphysical structure of the aerosol layer using instruments installed on a cable car was applied. Measurements on the cable car were enriched by continuous measurements performed at the LMS, UMS, and on three cable car supports. Frequent probing in time and space allowed for the determination of changes in the vertical distribution of aerosols.

The results indicate significant changes in aerosol mass concentration (total and eBC) with altitude only in the morning hours. In the noon and afternoon hours, the changes with altitude are significantly smaller and indicate stronger mixing of vertical air masses. Despite relatively stable meteorological conditions with no frontal zone, the observed changes in the vertical structure of the aerosol are visible at the 30-min interval. This demonstrates the mixing processes that occur, despite the stable stratification of the lower troposphere. This can be explained by the circulation of the mountain and valley breezes. Duan et al. (2021) reported that such circulation impacted the aerosol vertical distribution, particularly under weak weather conditions. The PM_{10} and eBC profiles show similar vertical variability, which can be explained by the altitude-independent aerosol composition. Observations at the LMS indicate relatively small intensive aerosol parameter variability, for example, SSA, which corresponds to negligible temporal variability of aerosol chemical composition, especially the contribution of absorbing particles. It should be emphasised that the lack of profiling overnight is a major limitation of the study of aerosol changes in a daily cycle, in particular, the development of surface night inversion and increase in aerosol concentration.

Profiling using the Microtops sun photometer showed that almost half of the AOD was present in the first 500 m of the atmosphere. In addition, vertical profiles of the AOD obtained during cable car soundings can be used to obtain the aerosol extinction coefficient at several wavelengths. Markowicz and Chilinski (2020) reported that the aerosol scattering coefficient can be estimated from low-cost aerosol counters,

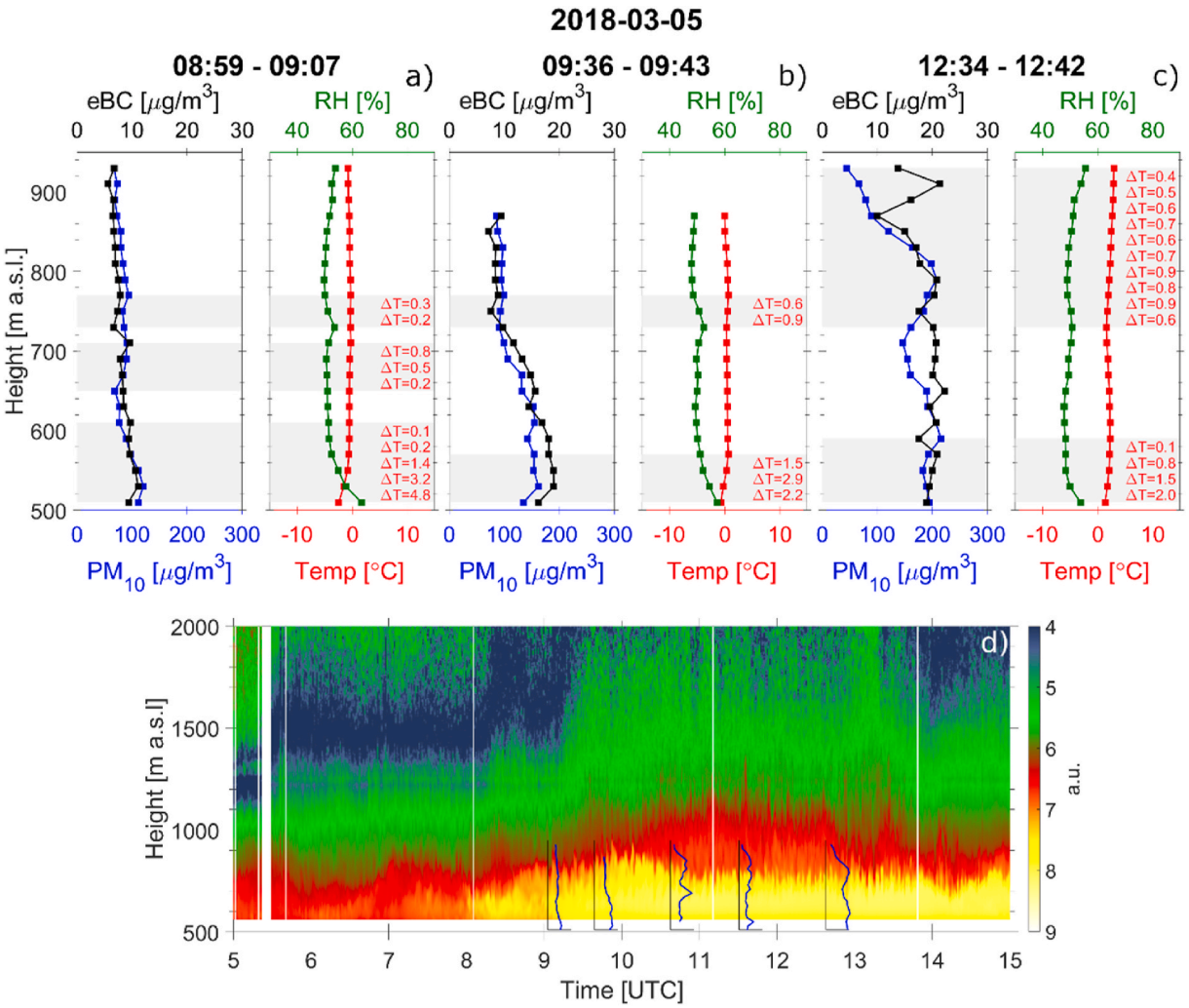

Fig. 9. Vertical profiles of PM_{10} in [μg/m^3] (blue line), eBC mass concentration in [μg/m^3] (black line), air temperature in [°C] (red line), and relative humidity in [%] obtained during cable car soundings on Mar 3, 2018 between (a) 08:59–09:07 UTC, (b) 09:36–09:43 UTC, and (c) 10:50–11:02 UTC. Logarithm of range-corrected lidar signal (at 1064 nm) registered on Mar 5, 2018 (d). Additional lines correspond to PM_{10} mass concentration profiles. (For interpretation of the references to colour in this figure legend, the reader is referred to the Web version of this article.)

for example, OPC-N2 and PMS7003 measurements. In future research, the vertical profiles of aerosol optical properties from the lidar and the low-cost aerosol counters, and the hand-held sun photometer onboard the cable cars could also be obtained and compared.

Observations in the LMS indicate that ground-to-air inversion is the main factor influencing the level of air pollution. In the first phase of the study, although the air temperatures were the lowest, probably because low emissions from the heating systems reached the highest values, the extensive parameters of the aerosol were not the highest. At that time, due to the relatively high pressure gradient, no nocturnal inversions developed, and the mixing of the air was intense. In the second phase, the air temperature was significantly higher (smaller emissions), but there were nocturnal inversions, which also continued during the day. This resulted in several times higher values of extensive parameters with relatively constant intensive values.

Credit author statement

M. A. Posyniak: Conceptualization, Software, Writing- Reviewing and Editing K. M. Markowicz: Methodology, Writing- Reviewing and Editing D. Czyzewska: Writing- Reviewing and Editing. M.T. Chilinski: Software P. Makuch Data curation O. Zawadzka-Manko Visualization, Data curation. S. Kucieba Writing, K. Kulesza Visualization, K. Kachniarz Writing K. Mijal: Data curation, K. Borek: Data curation.

Declaration of competing interest

The authors declare that they have no known competing financial interests or personal relationships that could have appeared to influence the work reported in this paper.

Acknowledgments

This research was conducted as part of the implementation of the National Science Centre projects no. 2016/23/D/ST10/03079 coordinated by the IG PAS and 2012/05/E/ST10/01578 coordinated by the IGP UW.

The authors thank the management of ZIAD Bielsko-Biala and the management and employees of the Szyndzielnia Cable Car for their cooperation in conducting the experiment. We also thank the workshop participants: Daria Bilinska, Wiktoria Czuchraj, Anetta Drzeniecka-Osiadacz, Marek Kowalczyk, Michal Kusmirek, Kornelia Miernik, Piotr Modzel, Tymoteusz Sawinski, and Gabriel Stachura.

Appendix A. Supplementary data

Supplementary data to this article can be found online at https://doi.org/10.1016/j.apr.2021.101171.

References

Bates, T.S., Quinn, P.K., Johnson, J.E., Corless, A., Brechtel, F.J., Stalin, S.E., et al., 2013. Measurements of atmospheric aerosol vertical distributions above Svalbard, Norway, using unmanned aerial systems (UAS). Atmos. Meas. Tech. 6 (8), 2115–2120.

Bulot, F.M., Johnston, S.J., Basford, P.J., Easton, N.H., Apetroaie-Cristea, M., Foster, G. L., et al., 2019. Long-term field comparison of multiple low-cost particulate matter sensors in an outdoor urban environment. Sci. Rep. 9 (1), 1–13.

Collaud Coen, M., Weingartner, E., Apituley, A., Ceburnis, D., Fierz-Schmidhauser, R., Flentje, H., et al., 2010. Minimizing light absorption measurement artifacts of the Aethalometer: evaluation of five correction algorithms. Atmos. Meas. Tech. 3, 457–474.

Chilinski, M.T., Markowicz, K.M., Markowicz, J., 2016. Observation of vertical variability of black carbon concentration in lower troposphere on campaigns in Poland. Atmos. Environ. 137, 155–170.

Chilinski, M.T., Markowicz, K.M., Kubicki, M., 2018. UAS as a support for atmospheric aerosols research: case study. Pure Appl. Geophys. 175, 3325–3342.

Chilinski, M.T., Markowicz, K.M., Zawadzka, O., Stachlewska, I.S., Lisok, J., Makuch, P., 2019. Comparison of columnar, surface, and UAS profiles of absorbing aerosol optical depth and single-scattering albedo in south-east Poland. Atmosphere 10 (8), 446.

Cheng, Y.H., Lin, M.H., 2013. Real-time performance of the microAeth® AE51 and the effects of aerosol loading on its measurement results at a traffic site. Aerosol Air Qual. Res. 13 (6), 1853–1863.

Colbeck, I., Lazaridis, M., 2010. Aerosols and environmental pollution. Naturwissenschaften 97, 117–131.

Devara, P.C.S., 1998. Review article Remote sensing of atmospheric aerosols from active and passive optical techniques. Int. J. Rem. Sens. 19 (17), 3271–3288.

Duan, J., Chen, Y., Wang, W., Li, J., Zhang, X., Lu, G., et al., 2021. Cable-car measurements of vertical aerosol profiles impacted by mountain-valley breezes in Lushan Mountain, East China. Sci. Total Environ. 768, 144198.

Ferrero, L., Castelli, M., Ferrini, B.S., Moscatelli, M., Perrone, M.G., Sangiorgi, G., et al., 2014. Impact of black carbon aerosol over Italian basin valleys: high-resolution measurements along vertical profiles, radiative forcing and heating rate. Atmos. Chem. Phys. 14, 9641–9664.

Hansen, A.D.A., Rosen, H., Novakov, T., 1984. The aethalometer – an instrument for the real-time measurement of optical absorption by aerosol particles. Sci. Total Environ. 36, 191–196.

Hagler, G.S.W., Yelverton, T.L.B., Vedantham, R., Hansen, A.D.A., Turner, J.R., 2011. Post-processing method to reduce noise while preserving high time resolution in aethalometer real-time black carbon data. Aerosol Air Qual. Res. 11, 539–546.

Hara, K., Osada, K., Yamanouchi, T., 2013. Tethered balloon-borne aerosol measurements: seasonal and vertical variations of aerosol constituents over Syowa Station, Antarctica. Atmos. Chem. Phys. 13 (17), 9119–9139.

Juda-Rezler, K., Toczko, B., Degorska, A., Fraczkowski, T., Gierczak, T., Iwanek, J., et al., 2016. Pyły Drobne W Atmosferze. Kompendium Wiedzy O Zanieczyszczeniu Powietrza Pyłem Zawieszonym W Polsce. Biblioteka Monitoringu Środowiska, Główny Inspektorat Ochrony Środowiska, Warsaw.

Kok, G., Walker, J.W., Arnott, W.P., Arnold, I.J., Keady, P.B., 2010. Photoacoustic extinctiometer (PAX): a new instrument for measurement of climate-relevant optical properties of aerosols. In: Proceedings of the AAAR 29th Annual Conference, October 25-29, 2010, Portland, Oregon, USA, p. 154.

Li, J., Chen, H., Li, Z., Wang, P., Cribb, M., Fan, X., 2015. Low-level temperature inversions and their effect on aerosol condensation nuclei concentrations under different large-scale synoptic circulations. Adv. Atmos. Sci. 32, 898–908.

Li, J., Chen, H., Li, Z., Wang, P., Fan, X., He, W., et al., 2019. Analysis of low-level temperature inversions and their effects on aerosols in the lower atmosphere. Adv. Atmos. Sci. 36 (11), 1235–1250.

Liu, Y., Jia, R., Dai, T., Xie, Y., Shi, G., 2014. A review of aerosol optical properties and radiative effects. J. Meteorol. Res. 28 (6), 1003–1028.

Markowicz, K.M., Flatau, P.J., Kardas, A.E., Remiszewska, J., Stelmaszczyk, K., Woeste, L., 2008. Ceilometer retrieval of the boundary layer vertical aerosol extinction structure. J. Atmos. Ocean. Technol. 25 (6), 928–944.

Markowicz, K.M., Chilinski, M.T., Lisok, J., Zawadzka, O., Stachlewska, I.S., Janicka, L., et al., 2016. Study of aerosol optical properties during long-range transport of biomass burning from Canada to Central Europe in July 2013. J. Aerosol Sci. 101, 156–173.

Markowicz, K.M., Ritter, C., Lisok, J., Makuch, P., Stachlewska, I.S., Cappelletti, D., et al., 2017. Vertical variability of aerosol single-scattering albedo and equivalent black carbon concentration based on in-situ and remote sensing techniques during the iAREA campaigns in Ny-Ålesund. Atmos. Environ. 164, 431–447.

Markowicz, K.M., Zawadzka, O., Posyniak, M., Uscka-Kowalkowska, J., 2019. Long-term variability of aerosol optical depth in the Tatra Mountains region of the Central Europe. J. Geophys. Res. 124 (6), 3464–3475.

Markowicz, K.M., Chilinski, M.T., 2020. Evaluation of two low-cost optical particle counters for the measurement of ambient aerosol scattering coefficient and ångström exponent. Sensors 20 (9), 2617.

Madueño, L., Kecorius, S., Andrade, M., Wiedensohler, A., 2020. Exposure and respiratory tract deposition dose of equivalent black carbon in high altitudes. Atmosphere 11 (6), 598.

Morys, M., Mims III, F.M., Hagerup, S., Anderson, S.E., Baker, A., Kia, J., et al., 2001. Design, calibration, and performance of MICROTOPS II handheld ozone monitor and Sun photometer. J. Geophys. Res. Atmos. 106 (D13), 14573–14582.

Nakayama, T., Suzuki, H., Kagamitani, S., Ikeda, Y., Uchiyama, A., Matsumi, Y., 2015. Characterization of a three wavelength photoacoustic soot spectrometer (PASS-3) and a photoacoustic extinctiometer (PAX). J. Meteorol. Soc. Jpn. Ser. II 93 (2), 285–308.

Okamoto, S., Tanimoto, H., 2016. A review of atmospheric chemistry observations at mountain sites. Prog. in Earth and Planet. Sci. 3, 34.

Pang, X., Chen, L., Shi, K., Wu, F., Chen, J., Fang, S., et al., 2021. A lightweight low-cost and multipollutant sensor package for aerial observations of air pollutants in atmospheric boundary layer. Sci. Total Environ. 764, 142828.

Posyniak, M., Stacewicz, T., Miernecki, M., Jagodnicka, A.K., Malinowski, S.P., 2010. Multiwavelength micropulse lidar for atmospheric aerosol investigation. Opt. Appl. 40 (3), 623–632.

Posyniak, M., Malinowski, S.P., Stacewicz, T., Markowicz, K.M., Zielinski, T., Petelski, T., et al., 2011. Multiwavelength micropulse lidar in atmospheric aerosol study: signal processing. In: Proceedings SPIE 8182. Lidar Technologies, Techniques, and Measurements for Atmospheric Remote Sensing VII, September 19-22, 2011, Prague, Czech Republic, p. 818216.

Seidel, J., Ketzler, G., Bechtel, B., Thies, B., Philipp, A., Böhner, J., et al., 2016. Mobile measurement techniques for local and micro-scale studies in urban and topo-climatology. Erde 147 (1), 15–39.

Stein, A.F., Draxler, R.R., Rolph, G.D., Stunder, B.J., Cohen, M.D., Ngan, F., 2015. Noaa's hysplit atmospheric transport and dispersion modeling system. Bull. Am. Meteorol. Soc. 96 (12), 2059–2077.

Stelmaszczyk, K., Dell'Aglio, M., Chudzyński, S., Stacewicz, T., Wöste, L., 2005. Analytical function for lidar geometrical compression form-factor calculations. Appl. Opt. 44 (7), 1323–1331.

Wang, H., Sun, Z., Li, H., Gao, Y., Wu, J., Cheng, T., 2018. Vertical-distribution characteristics of atmospheric aerosols under different thermodynamic conditions in beijing. Aerosol Air Qual. Res. 18 (11), 2775–2787.

Wielgosinski, G., Czerwinska, J., 2020. Smog episodes in Poland. Atmosphere 11 (3), 277.

Zawadzka, O., Posyniak, M., Nelken, K., Markuszewski, P., Chilinski, M.T., Czyzewska, D., et al., 2017. Study of the vertical variability of the aerosol properties based on cable cars in-situ measurements. Atmos. Pollut. Res. 8 (5), 968–978.

Zieger, P., Fierz-Schmidhauser, R., Weingartner, E., Baltensperger, U., 2013. Effects of relative humidity on aerosol light scattering: results from different European sites. Atmos. Chem. Phys. 13 (21), 10609–10631.

Zhang, Z., Xu, X., Qiao, L., Gong, D., Kim, S.J., Wang, Y., et al., 2018. Numerical simulations of the effects of regional topography on haze pollution in Beijing. Sci. Rep. 8 (1), 5504.